Progress In Electromagnetics Research M, Vol. 18, 247–257, 2011

IMAGING OF SEPARATE SCATTERERS BY MEANS OF A MULTISCALING MULTIREGION INEXACT-NEWTON APPROACH

G. Oliveri [1], A. Randazzo [2], M. Pastorino [2], and A. Massa [1, *]

[1]ELEDIA Research Center, Department of Information Engineering and Computer Science, University of Trento, Via Sommarive 14, Trento 38050, Italy

[2]Department of Biophysical and Electronic Engineering, University of Genova, Via Opera Pia 11 A, Genov 16145, Italy

Abstract—The integration of the Iterative Multi-Scaling Multi-Region (*IMSMR*) procedure and the Inexact-Newton method (*INM*) is proposed within the contrast-field formulation of the inverse scattering problem. Thanks to its features, such an implementation is expected to effectively deal with the reconstruction of separated objects. A selected set of numerical results is presented to assess the potentialities of the *IMSMR-INM* method also in comparison with previous *INM*-based inversions.

1. INTRODUCTION AND MOTIVATION

Non-invasive and non-destructive testing applications [1, 2] including biomedical imaging [3–5], subsurface prospecting [6], and material characterization [7] require fast and reliable microwave imaging techniques [8–10]. The development of inverse scattering methodologies comply-ing with these requirements is a challenging task because of (*I*) the ill-posedness/ill-conditioning and (*II*) the non-linearity of the associated inverse problems [11]. As for the "local minima" issue, which is due to the *non-linear* nature of the inverse problem and the limited amount of information coming from the scattering data [21], the use of global optimization techniques [12–15], alternative problem formulations (e.g., *Contrast Source*, *Born*, or *Rytov* formulations [16–18]), and multi-resolution strategies [19, 20] has been proposed. On

Received 14 May 2011, Accepted 10 June 2011, Scheduled 15 June 2011

* Corresponding author: Andrea Massa (andrea.massa@ing.unitn.it).

the other hand, several direct and indirect regularization approaches have been developed to mitigate the *ill-posedness/ill-conditioning* of the inversion [22, 23].

A promising approach to simultaneously address the theoretical difficulties (*I*) and (*II*) has been recently introduced by integrating a regularization technique with a local-minima-mitigation approach [24, 25]. Indeed, the so-called Iterative Multi-Scaling Inexact-Newton method (*IMSINM*) approach exploits, on the one hand, the regularization features of the *INM* [23] and, on the other, the effectiveness of the multi-focusing scheme to achieve high resolutions while reducing or avoiding local minima [19, 20]. The reliability and the numerical efficiency of the arising methodology has been preliminary assessed in [24, 25]. Despite these good performances, only a single "focusing" region has been considered during the inversion [24, 25] and reduced performances are expected when dealing with separated scatterers.

The aim of this work is to extend the method in [24, 25] to effectively retrieve multiple non-connected objects. Towards this end, the approach in [20] is nested within the *INM* and, unlike [25], separated regions-of-interest are dealt with to yield an Iterative Multi-Scaling Multi-Region Inexact Newton method (*IMSMR-INM*, Section 2). Representative numerical results are then presented in Section 3 to point out the improvements achievable over the single-region implementation [24, 25].

2. OUTLINE OF THE *IMSMR-INM*

With reference to a two-dimensional *TM*-illuminated scenario, the following integral equations relate the scattered $[E_v^{scatt}(\mathbf{r}) \triangleq E_v^{tot}(\mathbf{r}) - E_v^{inc}(\mathbf{r})]$, the total $[E_v^{tot}(\mathbf{r})]$, and the incident $[E_v^{inc}(\mathbf{r})]$ fields to the dielectric properties of a set of unknown scatterers described by the contrast function distribution $\tau(\mathbf{r}) = \varepsilon_r(\mathbf{r}) - 1$ [19] [$\varepsilon_r(\mathbf{r})$ being the relative dielectric permittivity] and embedded in a free-space background, ε_0 and μ_0 being its permittivity and permeability, respectively,

$$E^{scatt}(\mathbf{r}_m^v) = -k_0^2 \int_\Omega \tau(\mathbf{r}') E_v^{tot}(\mathbf{r}') G(\mathbf{r}_m^v/\mathbf{r}') d\mathbf{r}', \quad \mathbf{r}_m^v \in C \tag{1}$$

$$E_v^{inc}(\mathbf{r}) = E_v^{tot}(\mathbf{r}) + k^2 \int_\Omega \tau(\mathbf{r}') E_v^{tot}(\mathbf{r}') G(\mathbf{r}/\mathbf{r}') d\mathbf{r}', \mathbf{r} \in \Omega \tag{2}$$

where $k_0 = \sqrt{\varepsilon_0 \mu_0}$, C is the measurement curve external to the investigation domain Ω and where M measurement points $\mathbf{r}_m^v$, $m = 1, \ldots, M$, are located. Moreover, $G_{2D}(\mathbf{r}/\mathbf{r}')$ is the $2D$ Green's

function [19] and the superscript $v (v = 1, \ldots, V)$ identifies the v-th direction of incidence of the probing monochromatic wave whose time-dependence $\exp(j2\pi ft)$ is assumed and omitted hereinafter. The objective of the reconstruction procedure is that of inverting (1) and (2) to find the unknown distributions of $\tau(\mathbf{r})$ and $E_v^{tot}(\mathbf{r})$ in Ω starting from the knowledge of $E_v^{inc}(\mathbf{r})$, $\mathbf{r}_{\in}\Omega$, and $E_v^{scatt}(\mathbf{r}_m)$, $\mathbf{r}_m^v \in C$.

To image effectively multiple objects, a generalization of the approach in [24] able to identify and zoom on different sub-regions of the domain is needed. Towards this end, Equations (1) and (2) are firstly rewritten in a more compact form as $\mathbf{F}\{\mathbf{u}\} = \mathbf{d}$, where $\mathbf{u} \triangleq [\tau(\mathbf{r}); E_v^{tot}(\mathbf{r}),\ v = 1, \ldots, V]^T$, $\mathbf{d} \triangleq [E_v^{scatt}(\mathbf{r}_m^v),\ v = 1, \ldots, V,\ m = 1, \ldots, M; E_v^{inc}(\mathbf{r}_n),\ v = 1, \ldots, V]^T$, and $\mathbf{F}$ is the Lipmann-Schwinger nonlinear scattering operator in (1) and (2) [24]. By partitioning at each step ($s = 1, \ldots, S$, s being the step index) of the multiscaling process the investigation domain into N (N being the number of degrees of freedom of the scattered field [21]) cells centered at $\mathbf{r}_n^{(s)} (n = 1, \ldots, N)$ [26], the following algebraic nonlinear equation is then obtained

$$\mathbf{P}^{(s)} \left\{ \mathbf{u}^{(s)} \right\} = \mathbf{F}^{(s)} \left\{ \mathbf{u}^{(S)} \right\} - \mathbf{d}^{(s)} = 0 \tag{3}$$

where $\mathbf{d}(s) \triangleq \left[E_v^{scatt}(\mathbf{r}_m^v),\ v = 1, \ldots, V,\ m = 1, \ldots, M;\ E_v^{inc}(\mathbf{r}^{(s)_n}), v = 1, \ldots, V,\ n = 1, \ldots, N \right]^T$, $\mathbf{u}^{(s)} \triangleq \left[\tau(r_n^{(s)}),\ n = 1, \ldots, N;\ E_v^{tot}\mathbf{r}_n^{(s)}, v = 1, \ldots, V,\ n = 1, \ldots, N \right]^T$, $\mathbf{F}^{(s)}$ being the discretized version of $\mathbf{F}$.

To solve (3) also taking into account the multi-region distribution of the unknown scatterers, the following operations are repeated:

- *Clustering* — It is aimed at computing the number $Q^{(s)}$ and the locations/sizes of the regions-of-interest (*RoIs*) where the scatterers have been estimated to lie and where the synthetic zoom will take place. Such a task is carried out by firstly binarizing the pixel representation of the estimated contrast profile by means of a thresholding procedure based on the "image" histogram-concavity analysis [20] and then applying a noise filtering. Finally, a "labeling" is performed to estimate the membership of each pixel either to the background or to one of the *RoIs* [20];
- *Retrieval* — It is devoted to retrieve the dielectric profiles in each of the $Q^{(s)}$ *RoIs*. Towards this end, the following nested phases are iteratively performed by solving (3) in a regularized sense (according to the *IN* method) until the retrieved profile $\mathbf{u}_I^{(s)}$ is found ("outer *IN* loop", $i = 1, \ldots, I$):
  -*Linearization.* A Taylor expansion of $\mathbf{P}^{(s)}\{\mathbf{u}^{(s)}\}$ around to $\mathbf{u}_i^{(s)} (\mathbf{u}_0^{(s)} = \mathbf{u}_I^{(s-1)})$ is computed and then truncated at the first

order to determine the linear approximation $\mathbf{L}_i^{(s)}\{\mathbf{u}^{(s)}\}$ [24];
- *Update.* The guess solution is updated ($\mathbf{u}_{i+1}^{(s)} \triangleq \mathbf{u}_i^{(s)} + \mathbf{h}_i^{(s)}$) by determining $\mathbf{h}_i$. Towards this end, the equation $\mathbf{L}_i^{(s)}\{\mathbf{u}_i^{(s)} + \mathbf{h}_i^{(s)} = 0$ is iteratively solved through K steps of a truncated Landweber procedure [27] ("inner *IN* loop");

- *Termination* — It is aimed at assessing whether a "stationary" reconstruction is yielded in each region. More specifically, the multistep process is terminated ($s = S_{opt}$) when (a) the number, the dimensions, and the locations of the *RoIs* are stationary [20] and (b) the qualitative reconstructions of the unknowns $\mathbf{u}_I^{(s)}$ is accurate [23].

3. NUMERICAL RESULTS

The potentialities and limitations of the *IMSMR-INM* are assessed against synthetically-generated data. More specifically, the so-called "*E-L*" has been taken into account. It is com-posed by two homogeneous dielectric objects [Fig. 1(a)] belonging to a square investigation domain of side $\ell = 24\lambda$ illuminated by $V = 2.4$ *TM* plane waves impinging from the angular directions $\vartheta_v = 2\pi(v-1)/V$, $v = 1, \ldots, V$. The scattered field has been synthetically computed through the Richmond method [26] at $M = 360$ positions uniformly distributed on the circular measurement region C of radius $\rho = 18\lambda$. The *Bare-INM*, the *IMS-INM*, and the *IMSMR-INM* inversions have been carried out by setting $K = I = 60$ and choosing the maximum number of multi-focusing steps equal to $S = 5$.

By considering weak scatterers ($\tau = 0.5$) and noiseless data, the results from the different *INM*-based approaches are shown in Figs. 1(b)–1(d). Although both the *Bare-INM* and the *IMS-INM* allow one to identify the presence and the positions of two different objects, the reconstruction accuracy as well as the capability to avoid artifacts of the *IMSMR-INM* turn out to be significantly enhanced. This is quantitatively confirmed by the values of the error figures in Table 1 and defined as $\xi_\alpha = \frac{1}{N_\alpha} \sum_{n=1}^{N_\alpha} |\tilde{\tau}(\mathbf{r}_n) - \tau(\mathbf{r}_n)|/|\tau(\mathbf{r}_n) + 1| (\alpha = tot, ext, int)$ where N_α is the number of discretization domain of the whole investigation domain ($\alpha = tot$), within the scatterer ($\alpha = int$) or in the background region ($\alpha = ext$). Moreover, $\tilde{\tau}$ and τ stand for the retrieved contrast and the actual one, respectively. As it can be noticed (Table 1), the *IMSMR-INM* yields a total error of about 47% of that from the *Bare-INM* and approximately 69% of that

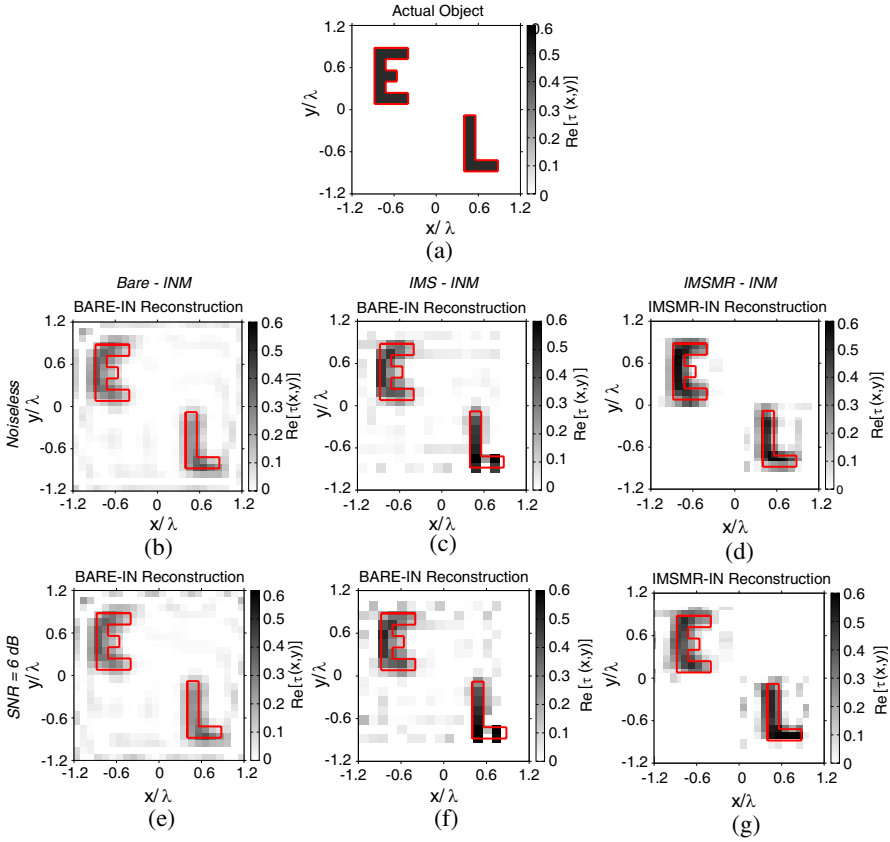

Figure 1. $[\tau = 0.5]$-Actual distribution (a) Reconstructed profile with (b)(e) the *Bare-INM*, (c)(f) the *IMS-INM*, and (d)(g) the *IMSMR-INM* in correspondence with (b)(c)(d) noiseless data and (e)(f)(g) noisy data ($SNR = 6\,\mathrm{dB}$).

Table 1. $[\tau = 0.5]$-Error and computational indexes.

	Noiseless				*SNR = 6 dB*			
Method	ξ_{tot}	ξ_{int}	ξ_{ext}	Δt [s]	ξ_{tot}	ξ_{int}	ξ_{ext}	Δt [s]
Bare	6.34×10^{-2}	1.63×10^{-1}	5.44×10^{-2}	5.40×10^{3}	6.90×10^{-2}	1.64×10^{-1}	6.04×10^{-2}	5.03×10^{3}
IMS−INM	4.33×10^{-2}	1.28×10^{-1}	3.57×10^{-2}	1.38×10^{3}	5.65×10^{-2}	1.38×10^{-1}	4.88×10^{-2}	1.33×10^{3}
IMSMR−INM	3.01×10^{-2}	1.00×10^{-1}	2.37×10^{-2}	1.28×10^{3}	4.66×10^{-2}	1.31×10^{-1}	3.89×10^{-2}	1.30×10^{3}

with the *IMS-INM* (i.e., $\xi_{tot}^{Bare} = 6.34 \times 10^{-2}$, $\xi_{tot}^{IMS} = 4.33 \times 10^{-2}$, $\xi_{tot}^{IMSMR} = 3.01 \times 10^{-2}$). Similar conclusions hold true for the internal ($\frac{\xi_{int}^{IMSMR}}{\xi_{int}^{Bare}} = 0.61$, $\frac{\xi_{int}^{IMSMR}}{\xi_{int}^{IMS}} = 0.78$) and the external ($\frac{\xi_{ext}^{IMSMR}}{\xi_{ext}^{Bare}} = 0.43$, $\frac{\xi_{ext}^{IMSMR}}{\xi_{ext}^{IMS}} = 0.92$) indexes, as well. For completeness, Fig. 2 and Table 2 give the evolution of the reconstructions and of the error metrics at different steps of the multi-resolution implementations of the *INM*, respectively.

As far as the robustness to the data noise is concerned, inversions of blurred data have been successively analyzed. The noise, which

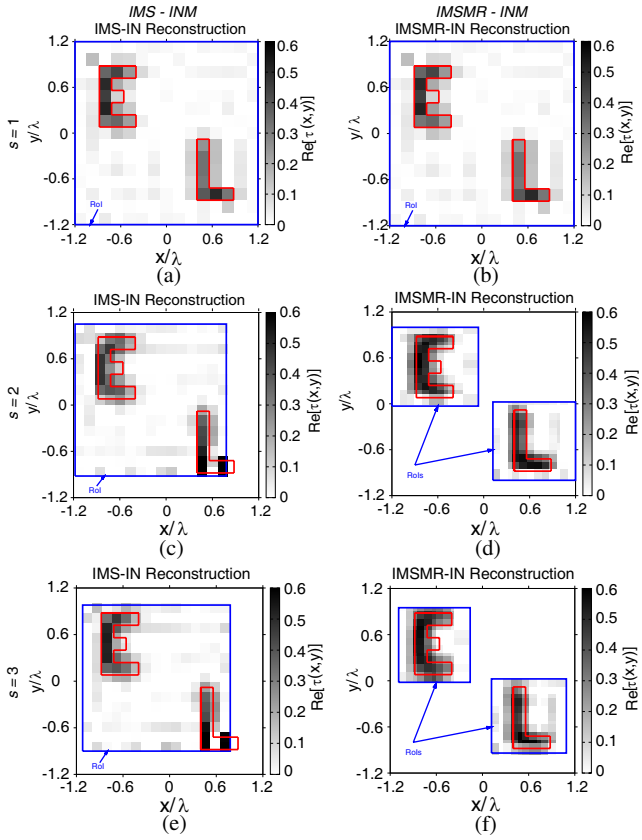

Figure 2. [$\tau = 0.5$, Noiseless data]-Evolution of the reconstruction at different steps [(a)(b) $s = 1$, (c)(d) $s = 2$, (e)(f) $s = S_{opt} = 3$] of the multi-resolution implementations of the *INM*: (a)(c)(e) *IMS-INM* and (b)(d)(f) *IMSMR-INM*.

Table 2. [$\tau = 0.5$, Noiseless Data]-Error indexes at different steps of the multi-focusing procedures.

	IMS- INM			*IMSMR- INM*		
s	ξ_{tot}	ξ_{int}	ξ_{ext}	ξ_{tot}	ξ_{int}	ξ_{ext}
1	4.71×10^{-2}	1.82×10^{-1}	3.48×10^{-2}	4.34×10^{-2}	1.02×10^{-1}	3.80×10^{-2}
2	4.68×10^{-2}	1.42×10^{-1}	3.82×10^{-2}	3.45×10^{-2}	0.98×10^{-1}	2.94×10^{-2}
3	4.33×10^{-2}	1.28×10^{-1}	3.57×10^{-2}	3.01×10^{-2}	1.00×10^{-1}	2.37×10^{-2}

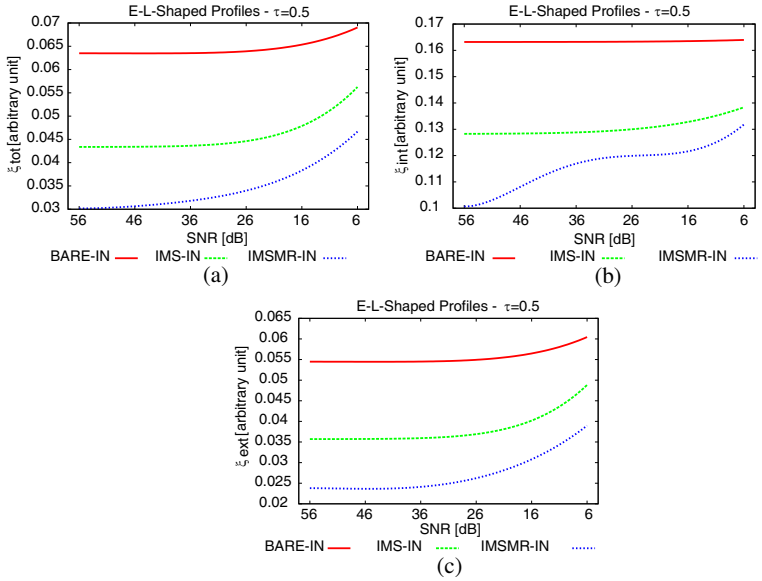

Figure 3. [$\tau = 0.5$]-Behavior of the error figures vs. *SNR*: (a) ξ_{tot}, (b) ξ_{int}, and (c) ξ_{ext}.

is characterized by a signal-to-noise ratio value, *SNR*, has been modeled by adding to the scattered field samples in C [i.e., $E_v^{scatt}(\mathbf{r}_m^v)$] randomly distributed values get from a Gaussian distribution. The plots of ξ_{tot} tot as a function of SNR [Fig. 3(a)] show that the accuracy of the *IMSMR-INM* degrades more significantly than that of the *INM* and the *IMS-INM* mainly for the worsening of the "external error" [Fig. 3(c)–Table 1]. This latter suggests that, as expected, some difficulties arise in estimating the extensions of

the different and separate *RoIs* when heavy noisy conditions verify. On the other hand, it cannot be neglected that the performances of the *MR* approach still overcome those from the other *INM* implementations as pictorially show in Figs. 1(e)–1(g) ($SNR = 6\,\text{dB}$) even though the inversion improvement ($\varsigma_o^{A-B} \triangleq (\xi_{tot}^A\rfloor_o - \xi_{tot}^B\rfloor_o)/\xi_{tot}^B\rfloor_o$) reduces from $\varsigma_{SNR=\infty}^{IMSMR-IMS} = 50\%$($\varsigma_{SNR=\infty}^{IMSMR-Bare} = 116\%$) down to $\varsigma_{SNR=26}^{IMSMR-IMS} = 34.6\%$($\varsigma_{SNR=26}^{IMSMR-Bare} = 95.5\%$) and $\varsigma_{SNR=6}^{IMSMR-IMS} = 20.5\%$($\varsigma_{SNR=6}^{IMSMR-Bare} = 47.9\%$).

With reference to the computational costs, the inversion time $\Delta t^{(1)}$ of the *MR* technique is close to that of the *IMS-INM* ($\Delta t^{IMSMR}/\Delta t^{IMS} \approx 0.95$-Table 1), while it is significantly shorter than that of the *INM* ($\Delta t^{IMSMR}/\Delta t^{Bare} \approx 0.24$-Table 1). As a matter of fact, a problem of the same size of the *IMS-INM* is solved at each step since the discretizations N_{IMS} and N_{IMSMR} only depend on the information available in the scattering data [21], while N_{INM} turns out to be larger because of the required fine resolution in Ω equal to that reached by the multiresolution procedures in the *RoIs* at S_{opt}.

To provide some more insights on the potentialities of the *MR* implementation, an analysis of the inversion accuracy versus the

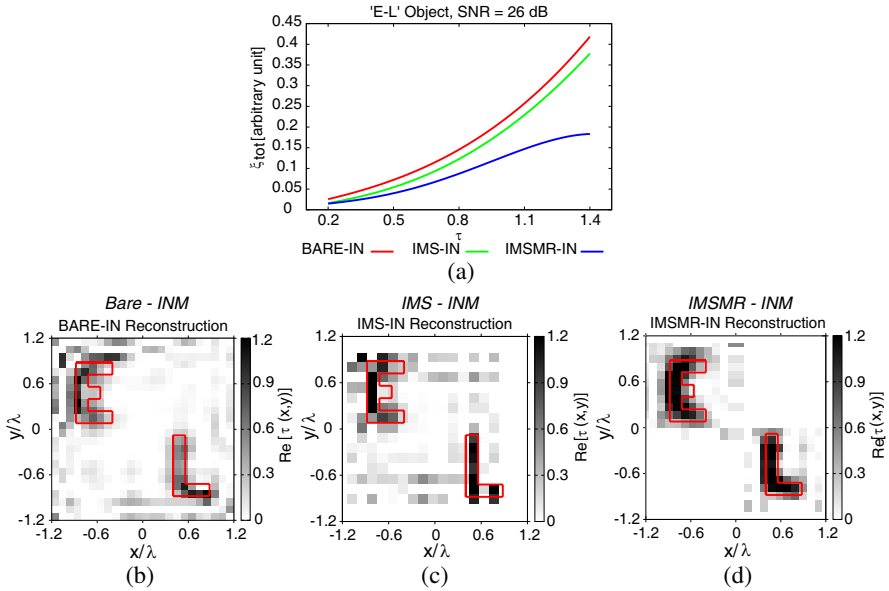

Figure 4. [$SNR = 26\,\text{dB}$] (a) Behavior of ξ_{tot} vs. τ. Reconstructions with (a) the *Bare-INM*, (b) the *IMS-INM*, and (c) the *IMSMR-INM* when $\tau = 1.1$.

dielectric properties of the scatterers has been carried out, as well. The actual contrast τ has been varied within the range $\tau \in [0.2, 1.4]$ and the scattered data have been blurred with a noise of $SNR = 26$ dB. The plots of the total reconstruction error as a function of the scatterers' contrast [Fig. 4(a)] indicate that: (a) the accuracy decreases for increasing contrasts whatever the *INM*-based method, (b) similar performances are yielded for low contrasts (e.g., $\varsigma_{\tau=0.2}^{IMSMR-IMS} = 91.4\%$), while (c) stronger scatterers are more carefully retrieved with the *IMSMR-INM* (e.g., $\varsigma_{\tau=1.1}^{IMSMR-IMS} = 71.6\%$) as also visually confirmed by the reconstructions in Figs. 4(b)–4(d) ($\tau = 1.1$).

4. CONCLUSION AND REMARKS

The retrieval of multiple separate scatterers in free space has been performed through an innovative version of the *IMS-INM*. Selected numerical results have been presented to assess the features, the potentialities, and limitations of the *IMSMR-INM* also in comparison with previous *INM* implementations. Future works will be aimed at further assessing the reliability of such an approach also against experimental data. An extension to three-dimensional problems is at present under investigation, as well.

REFERENCES

1. Giakos, G. C., et al., "Noninvasive imaging for the new century," *IEEE Instrum. Meas. Mag.*, Vol. 2, 32–35, Jun. 1999.
2. Zoughi, R., *Microwave Nondestructive Testing and Evaluation*, Kluwer Academic, Amsterdam, The Netherlands, 2000.
3. Caorsi, S., A. Massa, and M. Pastorino, "Numerical assessment concerning a focused microwave diagnostic method for medical applications," *IEEE Trans. Antennas Propag.*, Vol. 48, No. 11, 1815–1830, Nov. 2000.
4. Caorsi, S., A. Massa, M. Pastorino, and A. Rosani, "Microwave medical imaging: potentialities and limitations of a stochastic optimization technique," *IEEE Trans. Microwave Theory Tech.*, Vol. 52, No. 8, 1909–1916, Aug. 2004.
5. Zhou, H., T. Takenaka, J. Johnson, and T. Tanaka, "A breast imaging model using microwaves and a time domain three dimensional reconstruction method," *Progress In Electromagnetics Research*, Vol. 93, 57–70, 2009.
6. Chen, C.-C., J. T. Johnson, M. Sato, and A. G. Yarovoy, "Special

issue on subsurface sensing using ground-penetrating radar," *IEEE Trans. Geosci. Remote Sens.*, Vol. 45, No. 8, Aug. 2007.

7. Lesselier, D. and J. Bowler, "Special issue on electromagnetic and ultrasonic nondestructive evaluation," *Inverse Problems*, Vol. 18, No. 6, Dec. 2002.
8. Harada, H., D. J. N. Wall, T. Takenaka, and T. Tanaka, "Conjugate gradient method applied to inverse scattering problems," *IEEE Trans. Antennas Propag.*, Vol. 43, 784–792, Aug. 1995.
9. Ferraye, R., J. Y. Dauvignac, and C. Pichot, "Reconstruction of complex and multiple shape object contours using a level set method," *Journal of Electromagnetic Waves and Applications*, Vol. 17, No. 2, 153–181, 2003.
10. Dorn., O. and D. Lesselier, "Level set methods for inverse scattering," *Inverse Probl.*, Vol. 22, No. 4, Aug. 2006.
11. Colton, D. and R. Kress, *Inverse Acoustic and Electromagnetic Scattering Theory*, Springer-Verlag, Berlin Heidelberg, 1998.
12. Caorsi, S., A. Massa, and M. Pastorino, "A computational technique based on a real-coded genetic algorithm for microwave imaging purposes," *IEEE Trans. Geosci. Remote Sens.*, Vol. 38, No. 4, 1697–1708, Jul. 2000.
13. Donelli, M. and A. Massa, "A computational approach based on a particle swarm optimizer for microwave imaging of two-dimensional dielectric scatterers," *IEEE Trans. Microwave Theory Tech.*, Vol. 53, No. 5, 1761–1776, May 2005.
14. Pastorino, M., "Stochastic optimization methods applied to microwave imaging: A review," *IEEE Trans. Antennas Propag.*, Vol. 55, No. 3, 538–548, Mar. 2007.
15. Rocca, P., M. Benedetti, M. Donelli, D. Franceschini, and A. Massa, "Evolutionary optimization as applied to inverse scattering problems," *Inverse Probl.*, Vol. 25, No. 12, 1–41, Dec. 2009.
16. Van den Berg, P. M. and A. Abubakar, "Contrast source inversion method: State of the art," *Progress In Electromagnetics Research*, Vol. 34, 189–218, 2001.
17. Rocca, P., M. Donelli, G. L. Gragnani, and A. Massa, "Iterative multi-resolution retrieval of non-measurable equivalent currents for imaging purposes," *Inverse Probl.*, Vol. 25, No. 5, 1–25, May 2009.
18. Chen, X., "Subspace-based optimization method for solving inverse-scattering problems," *IEEE Trans. Geosci. Remote Sens.*,

Vol. 48, No. 1, 42–49, Jan. 2010.

19. Caorsi, S., M. Donelli, D. Franceschini, and A. Massa, "A new methodology based on an iterative multiscaling for microwave imaging," *IEEE Trans. Microwave Theory Tech.*, Vol. 51, No. 4, 1162–1173, Apr. 2003.
20. Caorsi, S., M. Donelli, and A. Massa, "Detection, location, and imaging of multiple scatterers by means of the iterative multiscaling method," *IEEE Trans. Microwave Theory Tech.*, Vol. 52, 1217–1228, Apr. 2004.
21. Bucci, O. M. and G. Franceschetti, "On the degrees of freedom of scattered fields," *IEEE Trans. Antennas Propag.*, Vol. 37, 918–926, Jul. 1989.
22. Mojabi, P. and J. LoVetri, "Overview and classification of some regularization techniques for the Gauss-Newton inversion method applied to inverse scattering problems," *IEEE Trans. Antennas Propag.*, Vol. 57, No. 9, 2658–2665, Sep. 2009.
23. Bozza, G., C. Estatico, A. Massa, M. Pastorino, and A. Randazzo, "Short-range imagebased method for the inspection of strong scatterers using microwaves," *IEEE Trans. Instrum. Meas.*, Vol. 56, No. 4, 1181–1188, Aug. 2007.
24. Oliveri, G., G. Bozza, A. Massa, and M. Pastorino, "Iterative multi scaling-enhanced inexact Newton-method for microwave imaging," *Proc. 2010 IEEE Antennas Propag. Soc. Int. Symp.*, 1–4, Toronto (Canada), Jul. 11–17, 2010.
25. Bozza, G., L. Lizzi, A. Massa, G. Oliveri, and M. Pastorino, "An iterative multi-scaling scheme for the electromagnetic imaging of separated scatterers by the Inexact-Newton method," *Proc. of the 2010 IEEE International Conference on Imaging Systems and Techniques (IST)*, 85–89, Thessaloniki, Greece, Jul. 1–2, 2010.
26. Richmond, J. H., "Scattering by a dielectric cylinder of arbitrary cross shape," *IEEE Trans. Antennas Propag.*, Vol. 13, No. 3, 334–341, May 1965.
27. Landweber, L., "An iteration formula for Fredholm integral equations of the first kind," *American Journal of Mathematics*, Vol. 73, No. 3, 615–624, Jul. 1951.